

# Advanced dynamic-equilibrium model for a nanobubble and a micropancake on a hydrophobic or hydrophilic surface

Kyuichi Yasui,\* Toru Tuziuti, Wataru Kanematsu, and Kazumi Kato

*National Institute of Advanced Industrial Science and Technology (AIST), 2266-98 Anagahora, Shimoshidami, Moriyama-ku, Nagoya 463-8560, Japan*

(Received 15 October 2014; published 16 March 2015)

The dynamic-equilibrium model for stabilization of a nanobubble on a hydrophobic surface by Brenner and Lohse [M. P. Brenner and D. Lohse, *Phys. Rev. Lett.* **101**, 214505 (2008)] has been modified taking into account the van der Waals attractive force between gas molecules inside a nanobubble and solid surface. The present model is also applicable to a nanobubble on a hydrophilic surface. According to the model, the pressure inside a nanobubble is not spatially uniform and is relatively higher near the solid surface. As a result, there is gas outflux near a hydrophilic surface, while near a hydrophobic surface there is gas influx which has been already suggested. In the present model, the radius of curvature for a nanobubble depends on the distance from the solid surface because the pressure depends on it. The shape of the micropancake, which is a nearly-two-dimensional bubble, is reproduced by the present model due to the strong dependence of the radius of curvature on the distance from the solid surface. The effect of temperature on the stability of a nanobubble or micropancake is also discussed.

DOI: [10.1103/PhysRevE.91.033008](https://doi.org/10.1103/PhysRevE.91.033008)

PACS number(s): 47.55.dr, 47.55.db, 68.47.—b

## I. INTRODUCTION

Following the suggestion by Parker *et al.* in 1994 [1] on the presence of stable nanobubbles on a hydrophobic surface, they have been directly observed with scanning atomic force microscopy (AFM) since 2000 [2–10]. Nanobubbles are usually formed by the exchange of a short-chain alcohol with water on a solid substrate called the standard solvent exchange procedure [6,11,12]. The reason for the nanobubble formation is the supersaturation of water with gas because the solubility of gas (air) in short-chain alcohol is about one order of magnitude larger than that in water. The evidence for the gas state inside a nanobubble has been experimentally reported by Zhang *et al.* [6,13] by the observation of rotational fine structure in the infrared (IR) spectrum of CO<sub>2</sub> and D<sub>2</sub>O. The average gas pressure inside a nanobubble was estimated from the IR spectrum as 1–2 atm. In addition, surface-plasmon resonance measurements revealed a lower refractive index of nanobubbles than water, which provides supporting evidence that the nanobubbles are in the gas state [6].

A nanobubble on a solid surface (surface nanobubble) has the shape of a lens with the height of several to several tens of nanometers and the lateral diameter of about 1 μm [10,14]. It means that the radius of curvature of a nanobubble is typically less than 1 μm. Then, the internal pressure is higher than 2.4 atm [ $p = p_0 + 2\sigma/R$ , where  $p_0$  is the liquid pressure (1 atm),  $\sigma$  is the surface tension ( $7.3 \times 10^{-2}$  N/m for water at 20 °C),  $R$  is the radius of curvature, and  $2\sigma/R$  is called the Laplace pressure]. The normal diffusion theory predicts the lifetime of a nanobubble is less than about 10 ms in gas-saturated water [15,16]. Nevertheless, the experimentally observed lifetime of a nanobubble was many orders of magnitude longer (more than 4 days for air bubbles and 1–2 hours for CO<sub>2</sub> bubbles) [6].

Several hypotheses have been proposed to explain the surprisingly long lifetime of surface nanobubbles [14,17–32].

One explanation is that the gas-water interface of a nanobubble is shielded by a layer of impermeable contamination [19]. It hinders diffusion of gases from a nanobubble, thereby increasing the lifetime. However, German *et al.* [29] experimentally showed that gas transfer actually took place across the surface of a nanobubble on a solid surface by measuring the rotational fine structure of CO<sub>2</sub> in the IR spectrum when nanobubbles formed in air-saturated water were perfused with CO<sub>2</sub>-saturated water. In another experiment, the CO<sub>2</sub> gas inside nanobubbles quickly dissolved into the surrounding air-saturated water, while nanobubbles remained stable for hours although CO<sub>2</sub> nanobubbles on a solid surface shrank upon exposure to air-saturated water. The observations clearly show that the gas inside surface nanobubbles is not sealed inside the bubbles.

Another explanation for the long lifetime of surface nanobubbles is based on the experimental fact that a three-phase (nanobubble-liquid-solid) contact line is strongly pinned on the solid surface (the pinning effect) due to the intrinsic nanoscale physical roughness or chemical heterogeneities of substrates [24,26,28,30,31,33,34]. Due to the pinning effect, the contact angle decreases as a surface nanobubble gradually dissolves into the liquid. In other words, the radius of curvature increases. It results in the decrease in the gas pressure inside a surface nanobubble, which strongly retards its dissolution into the liquid. There are also other kinds of theories on the long lifetime of a surface nanobubble based on the pinning effect [26,28]. In the present study, the pinning effect is simply taken into account by fixing the width of a surface nanobubble or a micropancake.

Furthermore, a different explanation for the long lifetime of surface nanobubbles was proposed by Brenner and Lohse [17] that the gas leaving the nanobubble is continuously replenished by the influx of gas near a hydrophobic surface because gas dissolved in the liquid is concentrated near a hydrophobic surface [35–40]. It is called the dynamic-equilibrium model. However, in this model, the attractive van der Waals potential is neglected between gas inside a nanobubble and the solid surface. In the present paper, the dynamic-equilibrium model

\*k.yasui@aist.go.jp

has been modified taking into account the potential. The modified model is applicable not only to a nanobubble on a hydrophobic surface but also to that on a hydrophilic surface, which has been experimentally observed [14,41–43].

A circulating liquid flow around a surface nanobubble has been believed to be responsible for the dynamic equilibrium [44]. However, such a flow was not experimentally detected in Refs. [43,45], and the dynamic-equilibrium model is currently criticized [46,47]. However, in the present model, the normal diffusion of gas in quiescent liquid is assumed, and the liquid flow is not necessarily required for the dynamic equilibrium.

Another mystery relating to surface nanobubbles is the mechanism of micropancake formation on a solid surface. Micropancakes are quasi-two-dimensional gaseous domains on a solid surface several microns in diameter but restricted to only 1–2 nm in height [41,42,48–53]. In most of the models for a nanobubble [54], a constant radius of curvature is assumed, and thus the shape of a micropancake could not be explained because the radius of curvature of a micropancake depends on the distance from the solid surface. In the present model, the gas pressure inside a bubble depends on the distance from the solid surface due to the van der Waals attractive potential between gas and a solid surface. According to the balance of the force on the bubble surface taking into account the Laplace pressure, the radius of curvature of the bubble surface depends on the distance from the solid surface in the present model. One of the objectives of the present paper is the application of the present model to a micropancake.

## II. MODEL

In the present model, the gas pressure inside a bubble on a solid surface is not spatially uniform. It depends on the distance from a solid surface irrespective of a hydrophobic or hydrophilic surface. The nonuniform gas pressure is due to the van der Waals attractive potential between a gas molecule and the solid surface. Due to the attractive potential, some gas molecules are trapped near the surface and hence the density becomes higher near the solid surface. Accordingly, the gas pressure becomes higher near the solid surface. This phenomenon is similar to the higher pressure for lower altitude in the atmosphere due to the attractive gravitational potential between the Earth and the atmospheric gas [55].

In the present study, a nanobubble or a micropancake on a solid surface in water is assumed to consist of argon gas and water vapor as in the experiment of Seddon *et al.* [44]. The shape of a nanobubble or a micropancake is assumed as axisymmetric with respect to the  $z$  axis for simplicity (Fig. 1). The width (diameter) of a nanobubble or a micropancake at a solid surface is fixed in the present numerical calculations as 700 nm, which was observed in the experiment [44], considering the pinning effect.

The van der Waals attractive potential between a pair of molecules as well as the strong repulsive one in close proximity of a molecule is expressed by the Lennard-Jones potential [ $w(r)$ ] [56]:

$$w(r) = \frac{A}{r^{12}} - \frac{B}{r^6}, \quad (1)$$

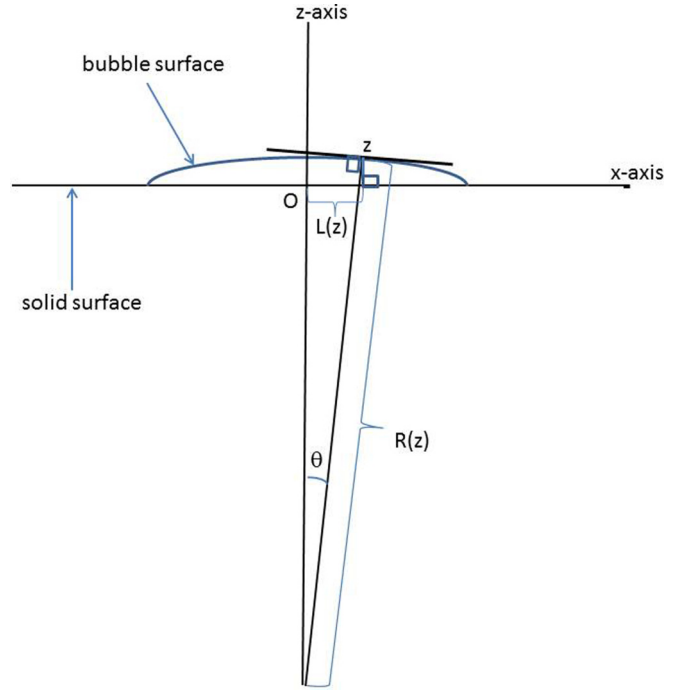


FIG. 1. (Color online) The definition of the symbols in the calculation for a nanobubble or a micropancake.

where  $A$  and  $B$  are constants, and  $r$  is the distance between a pair of molecules. The Lennard-Jones potential [ $w(z)$ ] between a gas (or vapor) molecule and a solid surface is expressed as follows [56]:

$$w(z) = \frac{\pi A \rho}{45z^9} - \frac{\pi B \rho}{6z^3}, \quad (2)$$

where  $z$  is the distance between a gas (or vapor) molecule and the solid surface, and  $\rho$  is the density of the solid. The constants  $A$  and  $B$  of the Lennard-Jones potential are related to the depth of the potential well ( $\varepsilon$ ) and the molecular diameter ( $d$ ) as follows:

$$A = 4\varepsilon d^{12}, \quad (3)$$

$$B = 4\varepsilon d^6. \quad (4)$$

In the present numerical calculations,  $A$  and  $B$  are assumed as follows using the typical values of  $\varepsilon = 0.005$  eV and  $d = 0.34$  nm [57]:  $A = 8 \times 10^{-135}$  J m<sup>12</sup> and  $B = 5 \times 10^{-78}$  J m<sup>6</sup>. The density of the solid is assumed as  $\rho = 1.1 \times 10^{29}$  m<sup>-3</sup> in number of atoms (molecules). The Lennard-Jones potential  $w(z)$  in Eq. (2) is shown in Fig. 2 normalized with  $k_B T$  where  $k_B$  is the Boltzmann constant and  $T$  is temperature which is assumed as 293 K (20 °C).

When the potential well is much wider than the mean free path of a gas molecule, the density of gas is proportional to  $\exp[-w(z)/k_B T]$  [55]. Accordingly, the gas (and vapor) pressure [ $p(z)$ ] is expressed as follows if the temperature is spatially uniform:

$$p(z) = \alpha e^{-\frac{w(z)}{k_B T}}, \quad (5)$$

where  $\alpha$  is a constant. The width of the well for the Lennard-Jones potential [Eq. (2)] is, however, only about 1 nm which

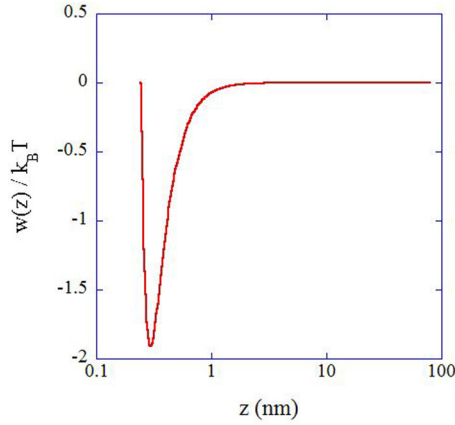


FIG. 2. (Color online) The Lennard-Jones potential between a gas molecule and a solid surface normalized with  $k_B T$  where  $k_B$  is the Boltzmann constant and  $T = 293$  K ( $20^\circ\text{C}$ ) is used. The horizontal axis ( $z$ ) is in logarithmic scale.

is more than an order of magnitude smaller than the mean free path of a gas molecule (about 20—100 nm) (Fig. 2). In this case, the actual gas (and vapor) pressure [ $\bar{p}(z)$ ] may be expressed as follows [58]:

$$\bar{p}(z) = f_t p(z) + \frac{1}{2}(1 - f_t) \int_{-\infty}^{\infty} p(z') \frac{e^{-|z'-z|/\bar{\lambda}_c}}{\bar{\lambda}_c} dz', \quad (6)$$

where  $f_t$  is the fraction of gas (and vapor) molecules trapped in the potential well when they come across the well, and  $\bar{\lambda}_c$  is the averaged mean free path of a gas (or vapor) molecule. In the present numerical calculations,  $f_t$  is assumed as 0.2 [59]. The mean free path of a gas (or vapor) molecule is estimated as follows [60]:

$$\bar{\lambda}_c = \frac{k_B T}{\sqrt{2S\bar{p}(z)}}, \quad (7)$$

where  $S$  is the cross section of a gas molecule and is assumed as  $3.6 \times 10^{-19}$  m<sup>2</sup> for argon. In the numerical calculations, the averaged mean free path  $\bar{\lambda}_c$  is estimated by Eq. (7) so as to be self-consistent with Eq. (6).

From Eq. (6), it is evident that the pressure inside a bubble depends on the distance  $z$  from the solid surface. Thus, the balance of pressure at the bubble surface is expressed as follows [61]:

$$\bar{p}(z) = p_0 + \sigma \left[ \frac{1}{R(z)} + \frac{1}{R'(z)} \right], \quad (8)$$

where  $p_0$  is the pressure in the liquid and is assumed as 1 atm,  $\sigma$  is the surface tension,  $R(z)$  is the radius of curvature of the bubble surface on the plane of Fig. 1, and  $R'(z)$  is that on the plane perpendicular to the plane of Fig. 1. In the present numerical calculations, however, the following approximation is employed:

$$\bar{p}(z) = p_0 + \frac{2\sigma}{R(z)}. \quad (8')$$

The maximum error associated with this approximation ranges from 35% to 50% in the value of  $R(z)$  near  $z = 0$ . Nevertheless, the range of  $z$  for the considerable error in

$R(z)$  is only about 0.5 nm according to the present numerical calculations. It means that the error is not important except for the case of a micropancake. This approximation may considerably overestimate the thickness of a micropancake. Numerical simulations of free-surface flows taking into account two different principal radii of curvature can be found in Ref. [62].

The shape of a nanobubble (or a micropancake) is calculated using  $R(z)$  as follows (Fig. 1):

$$dz = R(z) \sin \theta d\theta = \frac{R(z) \sin \theta dL}{|R(z)| \cos \theta}, \quad (9)$$

where  $(dL, dz)$  is a small displacement along the bubble surface in the  $x$ - $z$  plane,  $L(z)$  is the width (radius) of a bubble at  $z$ , and  $\theta$  is the angle defined in Fig. 1. For the numerical calculation of Eq. (9), the following relationship is used: When  $R(z) > L(z)$ ,

$$\sin \theta = \frac{L(z)}{R(z)}, \quad (10)$$

$$\cos \theta = \sqrt{1 - (\sin \theta)^2}. \quad (11)$$

When  $R(z) \leq L(z)$ ,

$$\tan \theta = \frac{|dz|}{|dL|}. \quad (12)$$

Equations (10) and (11) are accurate. However, Eq. (12) is an approximation. This approximation is used only for the case of Fig. 3 because for the other cases  $R(z) > L(z)$  always holds. The error associated with this approximation [Eq. (12)] is not so important because the range of  $z$  for  $R(z) \leq L(z)$  is only about 0.5 nm while the height of a surface nanobubble in Fig. 3 is about 100 nm.

At  $z = 0$  on a solid surface, the width (radius) of a nanobubble or a micropancake is fixed as  $L(z = 0) = 350$  nm in the present numerical calculations considering the pinning effect as already mentioned.

The gas influx [ $j(z)$ ] per unit surface area of a bubble is estimated by the following equation [15]:

$$j(z) = D \frac{\rho_{\text{H}_2\text{O}} \{ p_{\text{dis}}(z) - [\bar{p}(z) - p_{\text{vapor}}(z)] \}}{K R(z)}, \quad (13)$$

where  $D$  is the diffusion coefficient of gas in the liquid ( $D = 1.46 \times 10^{-9}$  m<sup>2</sup>/s for argon in water),  $\rho_{\text{H}_2\text{O}}$  is the molar concentration of water ( $= 5.56 \times 10^4$  mol/m<sup>3</sup>),  $K$  is Henry's constant ( $= 5.52 \times 10^9$  Pa),  $p_{\text{dis}}(z)$  is the partial pressure of gas dissolved in the liquid at  $z$ , and  $p_{\text{vapor}}(z)$  is the saturated vapor pressure at  $z$ . When  $j(z) < 0$ , it is the outflux of the gas across the bubble surface. While the partial pressure of gas in the liquid  $p_{\text{dis}}$  is independent of  $z$  near a hydrophilic surface, it strongly depends on  $z$  near a hydrophobic surface due to the hydrophobic interaction between gas dissolved in water and the solid surface [35–40]. It is estimated by the following equation [25]:

$$p_{\text{dis}}(z) = p_{\text{dis},\infty} \exp[-\Phi(z)/k_B T], \quad (14)$$

where  $p_{\text{dis},\infty}$  is the partial pressure of gas dissolved in the liquid far from a hydrophobic surface, and  $\Phi(z)$  is the potential of

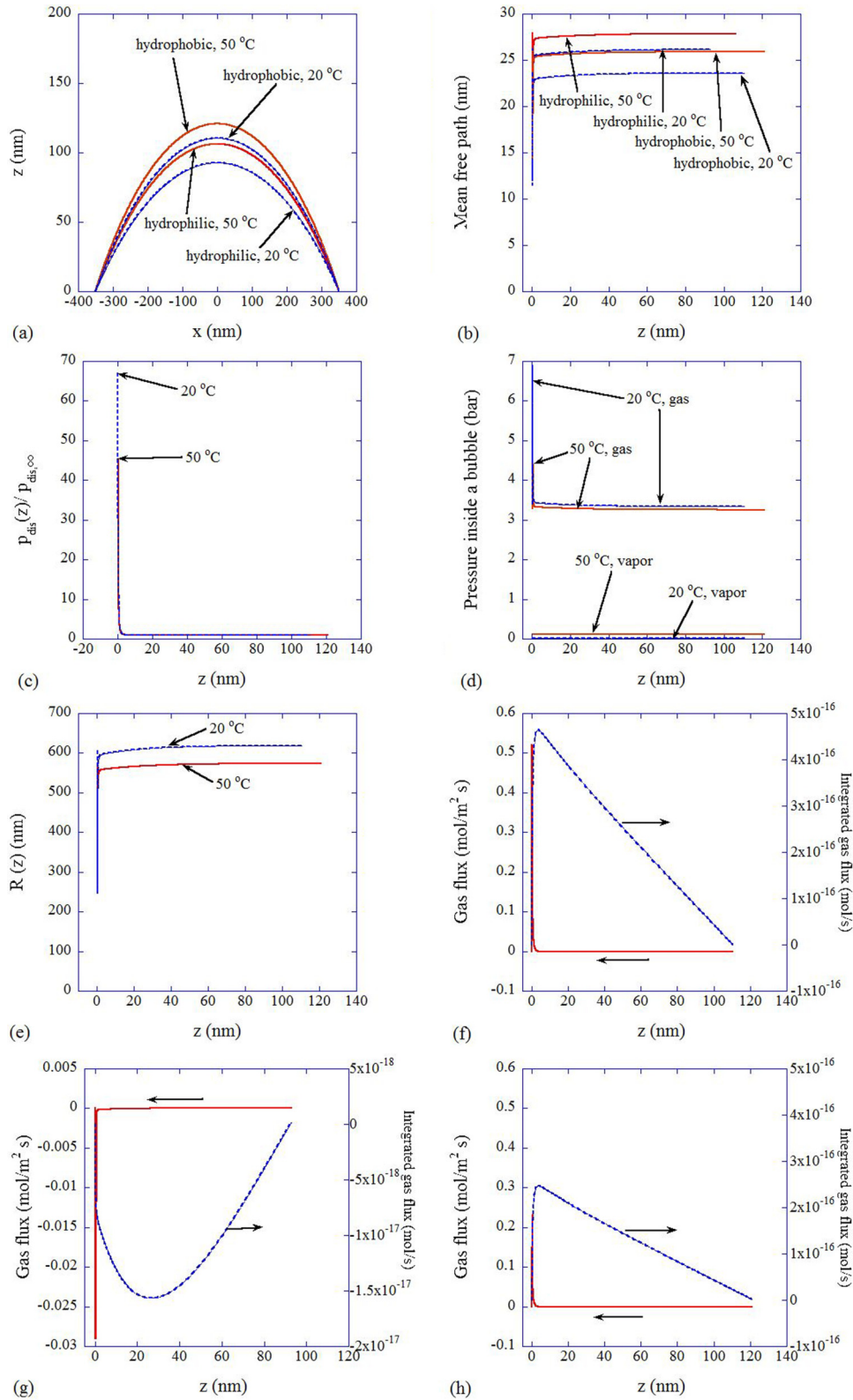


FIG. 3. (Color online) The calculated results for a nanobubble on a hydrophobic or hydrophilic surface in water supersaturated with 3 atm argon gas at 20 °C or 50 °C. The width (diameter) of a nanobubble is fixed as 700 nm. (a) The shape of a nanobubble. (b) The mean free path ( $\lambda_c$ ) of a gas molecule inside a nanobubble as a function of the distance ( $z$ ) from the solid surface. (c) The concentration of gas dissolved in liquid water as a function of the distance ( $z$ ) from a hydrophobic surface normalized with that far from the hydrophobic surface, which is equivalent to  $p_{\text{dis}}(z)/p_{\text{dis},\infty}$ . (d) The gas and vapor pressure inside a nanobubble on a hydrophobic surface as a function of  $z$ . (e) The radius of curvature ( $R$ ) for the shape of a nanobubble on a hydrophobic surface as a function of  $z$ . (f) The gas flux per unit surface area (solid line) and its surface integration (dotted line) from  $z = 0$  to  $z$  for a nanobubble on a hydrophobic surface at 20 °C. (g) Those for a nanobubble on a hydrophilic surface at 20 °C. (h) Those for a nanobubble on a hydrophobic surface at 50 °C.

the hydrophobic attraction given as follows:

$$\Phi(z) = -ae^{-bz}, \quad (15)$$

where  $a$  and  $b$  are constants. For a typical hydrophobic surface, the constants are as follows:  $a = 1.7 \times 10^{-20}$  J and  $b = 1 \text{ nm}^{-1}$  [25,56]. A particular surface of the solid is characterized by the constant  $a$ . As the constant  $a$  increases from 0 to about  $1.7 \times 10^{-20}$  J, a solid surface gradually changes from hydrophilic to hydrophobic. The border between hydrophilic and hydrophobic surfaces could be continuous. In the present paper, hydrophilic and hydrophobic surfaces are defined as  $a = 0$  and  $1.7 \times 10^{-20}$  J, respectively.

The saturated vapor pressure  $p_{\text{vapor}}(z)$  is a function of  $R(z)$  as follows [60]:

$$p_{\text{vapor}}(z) = p_{v,0} \exp[2\sigma V_m(l)/R(z)R_g T], \quad (16)$$

where  $p_{v,0}$  is the saturated vapor pressure at a flat liquid surface ( $=2.3 \times 10^3$  Pa at  $20^\circ\text{C}$ ,  $1.23 \times 10^4$  Pa at  $50^\circ\text{C}$ ),  $V_m(l)$  is the molar volume of liquid water ( $=1.8 \times 10^{-5}$  m<sup>3</sup>), and  $R_g$  is the universal gas constant ( $=8.31$  J/mol K). However, the variation of the saturated vapor pressure with  $R(z)$  is negligible for the range of  $R(z)$  in the present study.

The total gas influx ( $J$ ) across the bubble surface ( $surf$ ) is calculated as follows:

$$J = \int_{\text{surf}} 2\pi j(z)L(z)R(z)d\theta, \quad (17)$$

where  $d\theta$  is calculated as follows:

$$d\theta = \frac{dL}{R(z) \cos \theta}. \quad (18)$$

When  $J = 0$  with  $j(z) \neq 0$ , dynamic equilibrium of gas diffusion holds for a nanobubble or a micropancake. In other words, the gas influx is balanced with the gas outflux across the bubble surface in that case.

### III. RESULTS AND DISCUSSIONS

The present numerical calculations have been performed under a condition similar to that in the experiment by Seddon *et al.* [44]. In the experiment, the height and the width (diameter) of a nanobubble on freshly cleaved highly oriented pyrolytic graphite (HOPG) were about 90 and 700 nm, respectively, in water supersaturated with 3 atm argon gas. In the present numerical calculations, the width (diameter) is fixed as 700 nm considering the pinning effect. With regard to the height of a nanobubble, on the other hand, it is determined so as to make the total gas influx (or outflux) across the bubble surface vanish ( $J = 0$ ).

The results of the numerical calculations for nanobubbles in water supersaturated with 3 atm argon gas are shown in Fig. 3 both for hydrophobic ( $a = 1.7 \times 10^{-20}$  J) and hydrophilic surfaces ( $a = 0$ ) with temperatures of  $20^\circ\text{C}$  and  $50^\circ\text{C}$ . The height of a nanobubble is calculated as 93 nm and 110 nm at  $20^\circ\text{C}$  on hydrophilic and hydrophobic surfaces, respectively. The height is larger for a hydrophobic surface compared to a hydrophilic one. The value of the constant  $a$  for the freshly cleaved HOPG surface in the experiment is, however, unknown. In addition, there may be some error bar for the supersaturation pressure of 3 atm in the experiment. Thus it

may be practically very difficult to quantitatively compare the numerical results with the experimental data.

The height of a nanobubble at  $50^\circ\text{C}$  is larger than that at  $20^\circ\text{C}$  both on hydrophobic and hydrophilic surfaces in water supersaturated with 3 atm argon gas, while there is negligible effect of temperature on the height of a nanobubble in water saturated and undersaturated (degassed) with 1 atm and 0.8 atm argon gas, respectively [Figs. 3(a), 4, and 5(a)]. The larger height of a nanobubble at higher temperature has been experimentally reported [63].

The mean free path of a gas molecule inside a nanobubble is about 10–30 nm in water supersaturated with 3 atm argon gas [Fig. 3(b)]. Thus, the height of a nanobubble is about 4 times the mean free path in this case.

Near a hydrophobic surface, the gas concentration in liquid water is higher than that far from a hydrophobic surface by more than an order of magnitude due to the hydrophobic attraction between gas molecules dissolved in liquid water and the solid surface according to Eqs. (14) and (15) [Fig. 3(c)]. On the other hand, near a hydrophilic surface, it is independent of the distance from the solid surface, and the same as the gas concentration far from the solid surface.

Inside a nanobubble, on the other hand, gas pressure is higher by about a factor of 2 near a solid surface irrespective of a hydrophobic or hydrophilic surface due to the van der Waals attractive force between gas molecules and the solid surface according to Eq. (6) [Fig. 3(d)]. It should be noted, however, that the constants ( $A$  and  $B$ ) of the Lennard-Jones potential in Eq. (2) may depend on the hydrophobicity of the solid surface, and accordingly the gas pressure inside a nanobubble near the solid surface may also depend on it. The vapor pressure is nearly independent of the distance from the solid surface according to Eq. (16) because the radius of curvature [ $R(z)$ ] of the surface of a nanobubble is so large [Fig. 3(e)]. With regard to the dependence of surface tension on radius of curvature, it is negligible in the range of the radius of curvature for the surface of a nanobubble according to Tolman's equation [56].

Near a hydrophobic surface [ $z = 0$  in Fig. 3(f)], there is gas influx across the bubble surface due to the high concentration

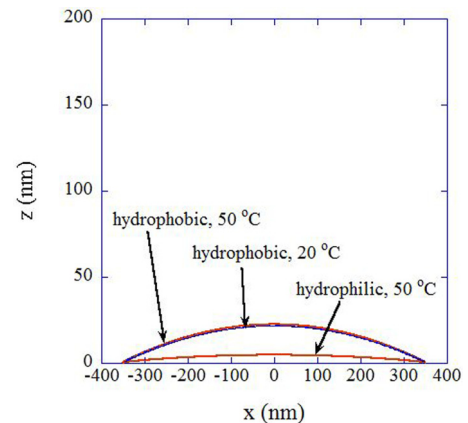


FIG. 4. (Color online) The calculated shape of a nanobubble on a hydrophobic or hydrophilic surface in water saturated with 1 atm argon gas at  $20^\circ\text{C}$  or  $50^\circ\text{C}$ . On a hydrophilic surface, there is no stable nanobubble at  $20^\circ\text{C}$ .

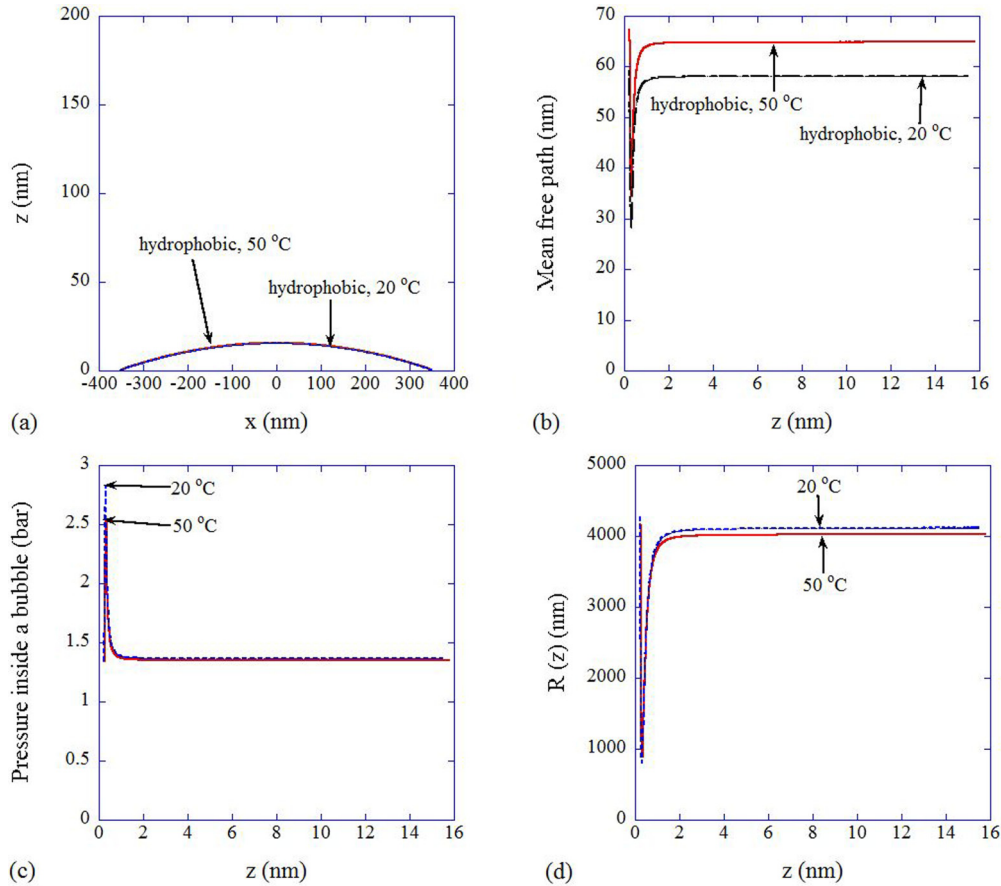


FIG. 5. (Color online) The calculated results for a nanobubble on a hydrophobic surface in water undersaturated with 0.8 atm argon gas at 20°C or 50°C. There is no stable nanobubble on a hydrophilic surface under the condition. (a) The shape of a nanobubble. (b) The mean free path ( $\lambda_c$ ) of a gas molecule inside a nanobubble. (c) The pressure inside a nanobubble [ $\bar{p}(z)$ ]. (d) The radius of curvature [ $R(z)$ ].

of gas dissolved in liquid water [Fig. 3(c)] as already suggested by Brenner and Lohse [17]. It balances with the gas outflux, which is seen by the surface integration of the gas influx (or outflux) vanishing at the top of a nanobubble at  $z = 110$  nm in Fig. 3(f). The dotted line in Figs. 3(f)–3(h) shows the surface integration of  $j(z)$  from  $z = 0$  to  $z$ . It gradually reaches 0 at the top of a nanobubble because gas influx and outflux are balanced under the conditions. On the other hand, near a hydrophilic surface [ $z = 0$  in Fig. 3(g)], there is gas outflux due to the higher gas pressure inside a nanobubble near the solid surface [Fig. 3(d)]. It balances with the gas influx as seen in Fig. 3(g). The average gas pressure inside a nanobubble on a hydrophilic surface is lower than that on a hydrophobic surface because there is gas outflux instead of influx near the solid surface which needs to be balanced with gas influx caused by the gas pressure inside a nanobubble being lower than the partial pressure of gas dissolved in the liquid. The lower gas pressure is the reason for the smaller height of a nanobubble on a hydrophilic surface compared to that on a hydrophobic surface.

As mentioned in the Introduction, the normal gas diffusion in a quiescent liquid is considered in the present model. Thus, the circulating liquid flow around a surface nanobubble is not necessarily required for the dynamic equilibrium. However, there may be some fluid (gas) flow inside a surface nanobubble according to the present model because the gradient of the van

der Waals potential is *not* precisely balanced with the pressure gradient inside a bubble due to Eq. (6). Further studies are required on this topic.

For 50°C, the saturated vapor pressure is much higher than that at 20°C [Fig. 3(d)]. As a result, the total pressure (gas + vapor) inside a nanobubble is higher than that at 20°C. It results in the larger height of a nanobubble at 50°C compared to that at 20°C in water supersaturated with 3 atm argon gas [Fig. 3(a)]. On the other hand, gas influx near a hydrophobic surface at 50°C is less than that at 20°C due to the lower gas concentration in the liquid near the hydrophobic surface [Fig. 3(c)]. This effect compensates for the previous one in water saturated or undersaturated with gas, and the height of a nanobubble on a hydrophobic surface is nearly independent of temperature in those cases [Figs. 4 and 5(a)].

On a hydrophilic surface in water saturated with 1 atm argon gas, a nanobubble is present only at relatively high temperature (50°C), and never present at 20°C because the gas pressure is so high at 20°C that there is only outflux of gas (Fig. 4). At 50°C, higher saturated vapor pressure causes lower gas pressure and consequently the gas influx. The presence of a nanobubble for lower concentration of gas in liquid water at higher temperature has been experimentally reported [52].

On a hydrophobic surface, a nanobubble is present in water undersaturated with 0.8 atm argon gas according to the present

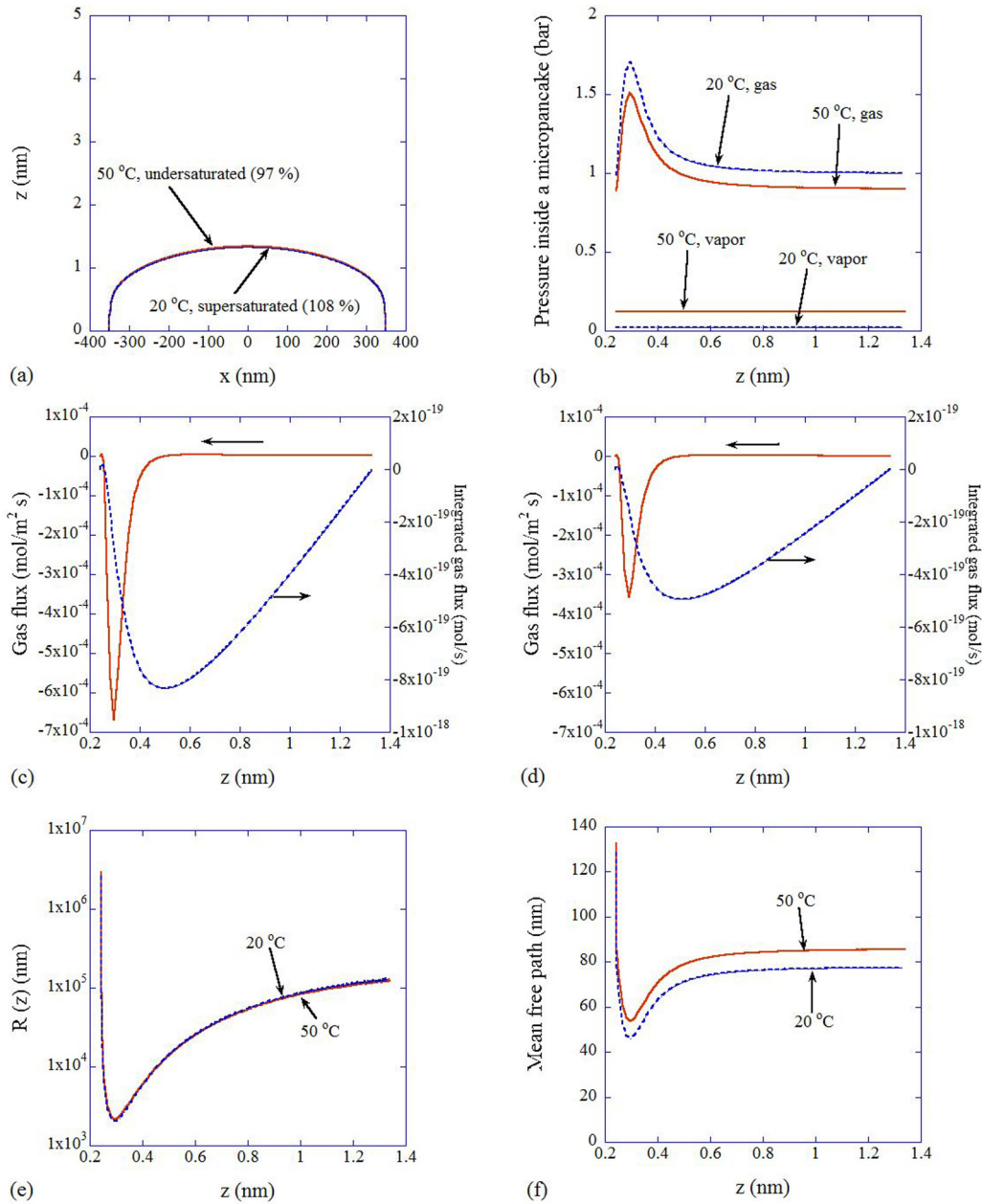


FIG. 6. (Color online) The calculated results for a micropancake on a hydrophilic surface in water supersaturated with 1.08 atm argon gas at 20 °C or undersaturated with 0.97 atm argon gas at 50 °C. The width (diameter) of a micropancake is fixed as 700 nm. (a) The shape of a micropancake. (b) The gas and vapor pressure inside a micropancake. (c) The gas flux per unit surface area of a micropancake (solid line) and its surface integration (dotted line) at 20 °C. (d) Those at 50 °C. (e) The radius of curvature  $[R(z)]$ . (f) The mean free path  $(\lambda_c)$  of a gas molecule inside a micropancake.

calculations [Fig. 5(a)]. On a hydrophilic surface, on the other hand, there is no stable nanobubble under the condition. The presence of surface nanobubbles in degassed water has been experimentally suggested [46,64]. The mean free path of a gas molecule inside a nanobubble under the condition is about 30–70 nm [Fig. 5(b)]. Thus the height of a nanobubble (15.5 nm) is much smaller than the mean free path in this case.

As the pressure inside a nanobubble depends on the distance  $(z)$  from a solid surface due to the van der Waals attractive potential between gas inside a nanobubble and the solid surface according to the present model, the radius of curvature  $[R(z)]$

of a nanobubble depends on  $z$  [Figs. 5(c) and 5(d)]. Thus, it is possible to calculate the shape of a micropancake based on the present model.

The calculated shape of a micropancake on a hydrophilic surface is shown in Fig. 6(a). The total gas influx (or outflux) vanishes for water supersaturated with 1.08 atm argon gas at 20 °C and that undersaturated with 0.97 atm argon gas at 50 °C. The gas pressure is lower than that in a nanobubble, which is the reason for the very small height (1.3 nm) of a micropancake [Figs. 3(d), 5(c), and 6(b)]. It should be noted, however, that the height of a micropancake could be considerably overestimated due to the approximation of Eq. (8'). The gas pressure inside a

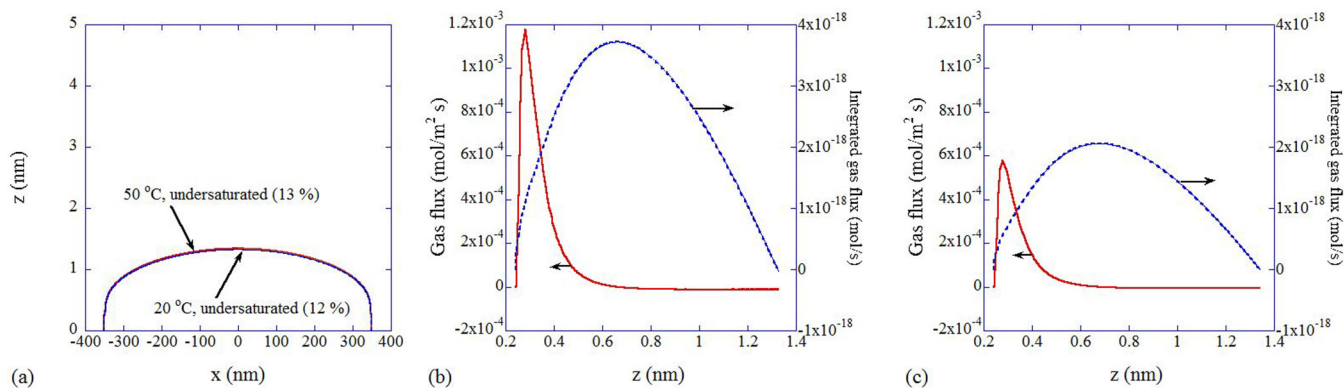


FIG. 7. (Color online) The calculated results for a micropancake on a hydrophobic surface in water undersaturated with 0.12 and 0.13 atm argon gas at 20 °C and 50 °C, respectively. (a) The shape of a micropancake. (b) The gas flux per unit surface area of a micropancake (solid line) and its surface integration (dotted line) at 20 °C. (c) Those at 50 °C.

micropancake on a hydrophilic surface at 50 °C is lower than that at 20 °C due to the higher saturated vapor pressure. In addition, the gas outflux near a hydrophilic surface is higher at 20 °C than that at 50 °C [Figs. 6(c) and 6(d)]. Accordingly, a micropancake of the same size is present for a lower gas concentration in liquid water at 50 °C compared to 20 °C.

As the gas pressure depends on  $z$ , the radius of curvature actually depends on  $z$ , which is the reason for the success in the reproduction of the shape of a micropancake [Figs. 6(b) and 6(e)]. The mean free path of a gas molecule is one or two orders of magnitude larger than the height of a micropancake [Fig. 6(f)].

Surprisingly, on a hydrophobic surface, a micropancake is present in highly degassed water according to the present model (Fig. 7). It is due to the gas influx near the hydrophobic surface [Figs. 7(b) and 7(c)]. As the gas influx at 20 °C is much higher than that at 50 °C due to higher gas accumulation near the hydrophobic surface, a micropancake is present for lower gas concentration in liquid water at 20 °C (12% in degree of gas saturation) compared to 50 °C (13%) although the average gas pressure is higher at 20 °C.

#### IV. CONCLUSION

The dynamic-equilibrium model proposed by Brenner and Lohse [17] has been modified taking into account the van

der Waals attractive potential between gas molecules inside a nanobubble and the solid surface. The present model is not only applicable to a nanobubble on a hydrophobic surface but also to that on a hydrophilic surface. In the present model, the gas pressure inside a surface nanobubble is not spatially uniform and is relatively higher near the solid surface due to the van der Waals attractive potential irrespective of a hydrophobic or hydrophilic surface. As a result, there is gas outflux near a hydrophilic surface, while there is gas influx near a hydrophobic surface due to the accumulation of gas dissolved in liquid water near the hydrophobic surface. The radius of curvature depends on the distance from the solid surface as the gas pressure depends on it. It makes the present model applicable to the quasi-two-dimensional bubble (micropancake). The present model suggests that a nanobubble or a micropancake could be present on a hydrophobic surface in highly degassed water. On a hydrophilic surface, on the other hand, a nanobubble or a micropancake could be present in slightly degassed water only at relatively high temperature.

#### ACKNOWLEDGMENTS

The authors would like to thank Dr. Yutaka Maruyama of AIST for useful discussions. A part of this work was supported by METI, Japan, as part of the international standardization project for fine bubbles.

- [1] J. L. Parker, P. M. Claesson, and P. Attard, *J. Phys. Chem.* **98**, 8468 (1994).
- [2] N. Ishida, T. Inoue, M. Miyahara, and K. Higashitani, *Langmuir* **16**, 6377 (2000).
- [3] S. T. Lou, Z. Q. Ouyang, Y. Zhang, X. J. Li, J. Hu, M. Q. Li, and F. J. Yang, *J. Vac. Sci. Technol. B* **18**, 2573 (2000).
- [4] N. Kameda and S. Nakabayashi, *Chem. Phys. Lett.* **461**, 122 (2008).
- [5] N. Kameda, N. Sogoshi, and S. Nakabayashi, *Surf. Sci.* **602**, 1579 (2008).
- [6] X. H. Zhang, A. Quinn, and W. A. Ducker, *Langmuir* **24**, 4756 (2008).
- [7] B. M. Borkent, S. de Beer, F. Mugele, and D. Lohse, *Langmuir* **26**, 260 (2010).
- [8] S. Nakabayashi, R. Shinozaki, Y. Senda, and H. Y. Yoshikawa, *J. Phys.: Condens. Matter* **25**, 184008 (2013).
- [9] C. W. Yang, Y. H. Lu, and I. S. Hwang, *J. Phys.: Condens. Matter* **25**, 184010 (2013).
- [10] B. Bhushan, Y. Pan, and S. Daniels, *J. Colloid Interface Sci.* **392**, 105 (2013).
- [11] X. Zhang, M. H. Uddin, H. Yang, G. Toikka, W. Ducker, and N. Maeda, *Langmuir* **28**, 10471 (2012).
- [12] X. Zhang, H. Lhuissier, O. R. Enriquez, C. Sun, and D. Lohse, *Langmuir* **29**, 9979 (2013).
- [13] X. H. Zhang, A. Khan, and W. A. Ducker, *Phys. Rev. Lett.* **98**, 136101 (2007).
- [14] J. R. T. Seddon, D. Lohse, W. A. Ducker, and V. S. J. Craig, *ChemPhysChem* **13**, 2179 (2012).

- [15] P. S. Epstein and M. S. Plesset, *J. Chem. Phys.* **18**, 1505 (1950).
- [16] K. Yasui, in *Sonochemistry and the Acoustic Bubble*, edited by F. Grieser, P. K. Choi, N. Enomoto, H. Harada, K. Okitsu, and K. Yasui (Elsevier, Amsterdam, 2015, in press).
- [17] M. P. Brenner and D. Lohse, *Phys. Rev. Lett.* **101**, 214505 (2008).
- [18] L. Zhang, H. Chen, Z. Li, H. P. Fang, and J. Hu, *Sci. China, Ser. G: Phys., Mech. Astron.* **51**, 219 (2008).
- [19] W. A. Ducker, *Langmuir* **25**, 8907 (2009).
- [20] J. H. Weijs, J. R. T. Seddon, and D. Lohse, *ChemPhysChem* **13**, 2197 (2012).
- [21] J. H. Weijs, J. H. Snoeijer, and D. Lohse, *Phys. Rev. Lett.* **108**, 104501 (2012).
- [22] N. F. Bunkin, A. V. Shkirin, P. S. Ignatiev, L. L. Chaikov, I. S. Burkhanov, and A. V. Starosvetskij, *J. Chem. Phys.* **137**, 054706 (2012).
- [23] N. F. Bunkin and A. V. Shkirin, *J. Chem. Phys.* **137**, 054707 (2012).
- [24] X. Zhang, D. Y. C. Chan, D. Wang, and N. Maeda, *Langmuir* **29**, 1017 (2013).
- [25] N. D. Petsev, M. S. Shell, and L. G. Leal, *Phys. Rev. E* **88**, 010402(R) (2013).
- [26] J. H. Weijs and D. Lohse, *Phys. Rev. Lett.* **110**, 054501 (2013).
- [27] H. Peng, G. R. Birkett, and A. V. Nguyen, *Langmuir* **29**, 15266 (2013).
- [28] Y. Liu and X. Zhang, *J. Chem. Phys.* **138**, 014706 (2013).
- [29] D. I. Zhukhovitskii, *J. Chem. Phys.* **139**, 164513 (2013).
- [30] Y. Liu, J. Wang, X. Zhang, and W. Wang, *J. Chem. Phys.* **140**, 054705 (2014).
- [31] Y. Liu and X. Zhang, *J. Chem. Phys.* **141**, 134702 (2014).
- [32] S. R. German, X. Wu, H. An, V. S. J. Craig, T. L. Mega, and X. Zhang, *ACS Nano* **8**, 6193 (2014).
- [33] A. Brotchie and X. H. Zhang, *Soft Matter* **7**, 265 (2011).
- [34] X. Zhang, H. Lhuissier, C. Sun, and D. Lohse, *Phys. Rev. Lett.* **112**, 144503 (2014).
- [35] A. Luzar and D. Bratko, *J. Phys. Chem. B* **109**, 22545 (2005).
- [36] S. M. Dammer and D. Lohse, *Phys. Rev. Lett.* **96**, 206101 (2006).
- [37] A. Poynor, L. Hong, I. K. Robinson, S. Granick, Z. Zhang, and P. A. Fenter, *Phys. Rev. Lett.* **97**, 266101 (2006).
- [38] D. Bratko and A. Luzar, *Langmuir* **24**, 1247 (2008).
- [39] M. Mezger, S. Schoder, H. Reichert, H. Schroder, J. Okasinski, V. Honkimaki, J. Ralston, J. Bilgram, R. Roth, and H. Dosch, *J. Chem. Phys.* **128**, 244705 (2008).
- [40] Y. H. Lu, C. W. Yang, and I. S. Hwang, *Langmuir* **28**, 12691 (2012).
- [41] X. Zhang and N. Maeda, *J. Phys. Chem. C* **115**, 736 (2011).
- [42] L. Zhang, C. Wang, R. Tai, J. Hu, and H. Fang, *ChemPhysChem* **13**, 2188 (2012).
- [43] C. U. Chan and C. D. Ohl, *Phys. Rev. Lett.* **109**, 174501 (2012).
- [44] J. R. T. Seddon, H. J. W. Zandvliet, and D. Lohse, *Phys. Rev. Lett.* **107**, 116101 (2011).
- [45] E. Dietrich, H. J. W. Zandvliet, D. Lohse, and J. R. T. Seddon, *J. Phys.: Condens. Matter* **25**, 184009 (2013).
- [46] R. P. Berkelaar, E. Dietrich, G. A. M. Kip, E. S. Kooij, H. J. W. Zandvliet, and D. Lohse, *Soft Matter* **10**, 4947 (2014).
- [47] C. Xu, S. Peng, G. G. Qiao, V. Gutowski, D. Lohse, and X. Zhang, *Soft Matter* **10**, 7857 (2014).
- [48] X. H. Zhang, X. Zhang, J. Sun, Z. Zhang, G. Li, H. Fang, X. Xiao, X. Zeng, and J. Hu, *Langmuir* **23**, 1778 (2007).
- [49] X. H. Zhang, N. Maeda, and J. Hu, *J. Phys. Chem. B* **112**, 13671 (2008).
- [50] L. Zhang, X. Zhang, C. Fan, Y. Zhang, and J. Hu, *Langmuir* **25**, 8860 (2009).
- [51] J. R. T. Seddon, O. Bliznyuk, E. S. Kooij, B. Poelsema, H. J. W. Zandvliet, and D. Lohse, *Langmuir* **26**, 9640 (2010).
- [52] J. R. T. Seddon, E. S. Kooij, B. Poelsema, H. J. W. Zandvliet, and D. Lohse, *Phys. Rev. Lett.* **106**, 056101 (2011).
- [53] J. R. T. Seddon and D. Lohse, *J. Phys.: Condens. Matter* **23**, 133001 (2011).
- [54] V. S. J. Craig, *Soft Matter* **7**, 40 (2011).
- [55] A. Sommerfeld, in *Thermodynamics and Statistical Mechanics*, edited by F. Bopp and J. Meixner, translated by J. Kestin (Academic Press, New York, 1964).
- [56] J. N. Israelachvili, *Intermolecular and Surface Forces*, 3rd ed. (Elsevier, Amsterdam, 2011).
- [57] Z. Shi, M. Barisik, and A. Beskok, *Int. J. Therm. Sci.* **59**, 29 (2012).
- [58] T. Einwohner and B. J. Alder, *J. Chem. Phys.* **49**, 1458 (1968).
- [59] R. M. Logan and J. C. Keck, *J. Chem. Phys.* **49**, 860 (1968).
- [60] P. W. Atkins, *Physical Chemistry*, 6th ed. (Oxford University Press, Oxford, 1998).
- [61] A. W. Adamson, *Physical Chemistry of Surfaces*, 5th ed. (John Wiley & Sons, New York, 1990).
- [62] J. Eggers, *Rev. Mod. Phys.* **69**, 865 (1997).
- [63] R. P. Berkelaar, J. R. T. Seddon, H. J. W. Zandvliet, and D. Lohse, *ChemPhysChem* **13**, 2213 (2012).
- [64] S. Wang, M. Liu, and Y. Dong, *J. Phys.: Condens. Matter* **25**, 184007 (2013).